Optimised Magnetic Design of Superconducting Magnets for Heavy-Ion Rotating Gantries

Optimised Magnetic Design of Superconducting Magnets for Heavy Ion Rotating Gantries

Yvonne T. E. Baird, Quan Li

School of Engineering, Institute for Energy Systems, The University of Edinburgh, United Kingdom
Corresponding author: Quan Li, email: Quan.Li@ed.ac.uk

***Abstract*—Superconductors enable extremely high field magnets that can be used to develop compact heavy-ion rotating gantries and accelerators. To achieve high fields, a large quantity of superconducting material is required. This results in high costs and difficulties on cooling. An effective design algorithm is necessary to optimize the magnet designs and reduce materials needed. In this paper, we propose a new design method for high temperature superconducting (HTS) magnets with combined function for carbon-ion therapy rotating gantries. The new method applies a layer-by-layer design process, which effectively reduces the total volume of superconducting material required and improves field precision. Firstly, the cross-section of a multilayer magnet was designed to achieve combined fields of dipole and quadrupole. Based on this, three-dimensional magnet coil ends were designed, considering mechanical constraints of the HTS coated conductors. Results show that the new design requires 26.3% less material than the existing design with a highly precise field strength and distribution.**

***Index Terms*—Coated conductor, gantry, magnet design, medical accelerator.**

I. Introduction

Treatment of cancerous tumours using charged particles continues to play an increasing role, however continuous efforts must be made in order to further develop particle radiotherapy, thus enabling this treatment form to become more widely available. The widespread use of carbon ion radiotherapy (CIRT) has been limited due to not only the costs associated with this treatment form, but also the size of the facilities. A rotating gantry is the most suited beam delivery method for CIRT, being able to deliver beams from any direction, whilst the patient is kept in the optimal position for treatment. Although a number of rotating gantries exist for proton therapy, only two rotating gantries currently exist for CIRT. Carbon beams with a kinetic energy of 430 MeV/u require a magnetic rigidity which is approximately three times larger than that required for proton beams, resulting in a large, and heavy structure [1]. Superconducting technology was used in the second carbon-ion rotating gantry, which was installed at the National Institute for Radiological Sciences (NIRS). Low temperature superconducting (LTS) combined function magnets were designed to overcome the problem of weight and size, which resulted in a rotating gantry of similar size as those used in proton therapy. The LTS combined function magnet has a layered structure. With a total of 34 layers, 400 turns/pole for the quadrupole coil and 3426 turns/pole for the dipole coil, the inner 8 layers are wound with a cos(2θ) distribution allowing a pure quadrupole field to be produced, the additional 26 layers wound on top have a cos(θ) distribution to produce a pure dipole field. A maximum field gradient of 9 T/m and a magnetic flux density of 2.88 T were achieved with this design [2].

It is however still highly desirable to further improve the design of the magnets for mass and volume reduction. In order to achieve this objective, the use of high temperature superconductors (HTS) in the design of combined function magnets have been studied and modelled in this paper. Compared to the characteristics of LTS, HTS possesses several advantages including: the generation of higher magnetic fields due to their high critical current densities; easy and efficient cooling through the use of a cryocooler; as well as improved thermal stability [3] - [4].

Another consideration which was taken into account throughout the design process was to design a HTS combined function magnet with an economical amount of HTS tape, due to the costs associated with superconducting tape [5] and losses even carrying DC current [6] - [10]. In this paper, unlike the previous designs, we propose a magnet design in which each individual layer can generate both dipole and quadrupole functions of bending and focusing/defocusing respectively. Instead of designing all layers simultaneously, this new layer-by-layer design uses space effectively. This optimised design enables further reduction of superconducting material compared to other known designs, thus more compact magnets with precise magnetic fields.

II. Applicability to Heavy-ion accelerators and rotating gantries

Straight superconducting combined function magnets achieving 2.88 T and 9.0 T/m have already been designed for accelerators, but as previously mentioned using a layered approach. The existing approach does not use space effectively like in this design, and therefore ends up costing more due to the volume of superconducting material used. Although gantry magnets tend to be a combination of superconducting curved magnets and straight normal conducting magnets, a combination of straight and curved superconducting combined function magnets could be a potential, particularly seeing how

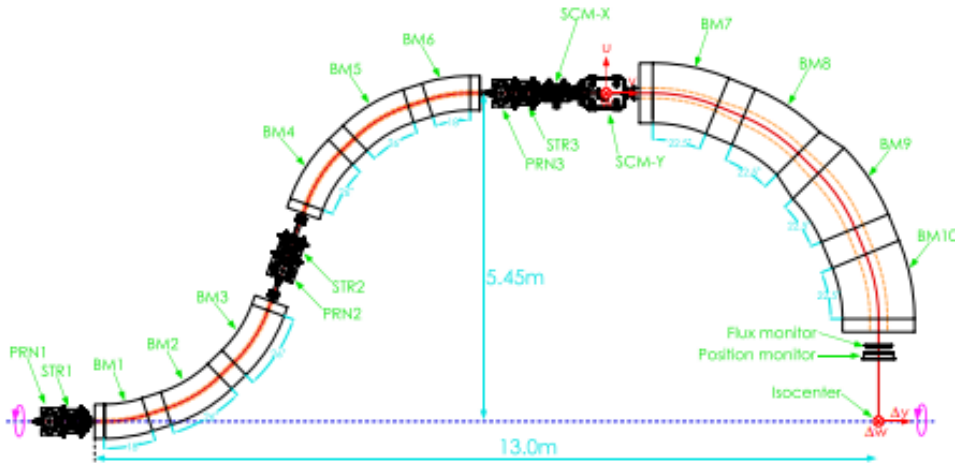

Fig. 1 Layout of the superconducting rotating gantry at NIRS [2].

new designs of the facility as a whole are being proposed, including multi-level facilities [11].

For example, straighter sections of the gantry beam line seen in Fig. 1, such as those represented by BM3 and BM4 designed with a field strength of 2.88 T and 9.0 T/m to be able to transport the carbon beam with energy of 430 MeV/u, [2] could be combined, and make use of the designed straight superconducting combined function magnet, in conjunction with short bending magnets if required.

A 'flattened' gantry design as in [12] and [13] utilising straighter sections to reduce the height of the gantry and supporting structures, could use a combination of straight and curved combined function magnets to achieve this.

III. COMBINED FUNCTION MAGNET DESIGN OVERVIEW

A. Design Concept: layer-by-layer design

Unlike the existing design methods for gantry magnets, we applied a layer-by-layer design algorithm to design each layer individually. This greatly reduces both material mass and volume. The HTS combined function magnet is designed using a 5 mm wide and 0.2 mm thick HTS tapes, aiming to achieve a dipole field of 2.88 T and a quadrupole field of 9.0 T/m [14]. Additional design specifications are listed in Table I. In the design of accelerator magnets it is common to take a reference radius that is approximately 2/3 of the magnet aperture, thus the reference radius of this magnet is set at 35 mm. The superconducting magnets BM1-BM6 installed on the rotating gantry at NIRS were also designed with this specification [2]. Due to the magnet being designed with x-axis symmetry, only normal field components exist that require minimising [15]. For each layer, the coils have been divided into a number of block-shaped windings in the azimuthal direction in order to reduce field harmonics of higher order [16]. The higher order harmonics were calculated at the center of the magnet's cross-section. Each space harmonic must be lower than 10^{-4} of the central field to ensure a homogeneous field, due to the requirement for good beam quality [17].

B. Magnetic Field and Multipole Components in the Magnet Cross-Section

It is important to describe the field quality in the magnet aperture in terms of harmonic multipole coefficients, which substantially affect the precision of the magnetic field required. The multipole coefficients are given in cylindrical coordinates as [15]

$$B_\theta(r,\theta) = \sum_{n=1}^{\infty}\left(\frac{r}{r_0}\right)^{n-1}\left(B_n(r_0)\cos n\theta - A_n(r_0)\sin(n\theta)\right), \quad (1)$$

$$B_r(r,\theta) = \sum_{n=1}^{\infty}\left(\frac{r}{r_0}\right)^{n-1}\left(B_n(r_0)\sin n\theta + A_n\cos(n\theta)\right), \quad (2)$$

where B_n and A_n are the normal and skew multipole components of the magnetic field, and r_0 is the reference radius.

TABLE I
DESIGN SPECIFICATIONS

Specification	Value	Unit
Radius of mandrel	50	mm
Inner radius of iron yoke	120	mm
Outer radius of iron yoke	270	mm
Separation between coated conductors	0.1	mm
Coated conductor thickness	0.2	mm
Superconductor layer thickness	2	µm
Width of coated conductor	5	mm
Operation current	200	A
Magnet straight section length	1	m
Reference radius	35	mm
Higher harmonics	$<10^{-4}$	-
Flat-wise bending radius	>20	mm
Edge-wise bending strain	<0.3	%

The iron yoke's influence was considered by the image current method [18], as in [19], [20], [4], and [21]. By using the image current method the iron is represented by an infinite outer boundary by means of image currents. Through summation of the field generated by the image currents and the applied field, the field in the problem domain can be calculated [18].

The current was considered to be a line current at the center of each turn of the coated conductor.

The Biot-Savart law was used to calculate the magnetic field generated by the image currents.
The image current's magnitude and position in the iron yoke is expressed as follows [20]:

$$r' = \frac{r_{iron}^2}{r}, \tag{3}$$

$$I' = I\,x(\mu_{iron} - 1)/(\mu_{iron} + 1), \tag{4}$$

where r_{iron}, r' and r are the distance from the z-axis to the iron yoke's inner surface, the image current, and to the real current, respectively. The magnitude of the real current in one turn and the image current of it is represented by I and I'. $\mu_{iron}$is the relative permeability of the iron yoke.
The normal multipole coefficients inside the magnet aperture for a line current can be determined from [22]:

$$B_n(r_0) = -\frac{\mu_0 I}{2\pi}\frac{r_0^{n-1}}{r_i^n}\left(1 + \frac{\mu_r - 1}{\mu_r + 1}\left(\left(\frac{r_i}{R_{yoke}}\right)^{2n}\right)\right)cos(n\vartheta). \tag{5}$$

This allows the field quality in the straight section of the magnet to be determined and takes into account the effect of the image currents mentioned for an iron yoke with radius $R_{yoke.}$
The iron yokes' influence is greater on the higher harmonic multipole coefficients than the lower order ones, and so optimization for higher harmonic multipole coefficients is important for accelerator magnet design. The contribution of the yoke on the harmonic multipole coefficients can be determined from [23]:

$$\frac{B_N^{imag}}{B_N + B_N^{imag}} \approx \left(1 + \left(\frac{r_y}{r}\right)^{2N}\right)^{-1}. \tag{6}$$

By adding the terms in (5) the harmonic content of a field generated by line-currents carrying current I at the position (r_i, ϑ_i) can be calculated.
Each multipole coefficient is generated by a surface current on the mandrel of the magnet, which can be calculated. The positions of the conductors are then be determined, and optimsed.
To ensure the required field quality is met, higher order normal 2n-pole components that have been normalised by the reference magnetic field - the dipole component B_1, are controlled to be less than 10^{-4}. The normal 2n-pole components are normalised as in (7) [3]

$$b_n = \frac{1}{B_{ref}} B_n. \tag{7}$$

C. Three-Dimensional Design

Designing and optimising superconducting magnets is difficult due to the various design constraints of the superconducting coated conductor. The constraints include inter-layer spacing, minimum bending radius, and other mechanical constraints. Due to the mechanical constraints, the coated conductors are hard to bend and wind, thus flat-wise bending, edge-wise bending, and torsion must be considered when designing the coil ends of the magnet.
The curved line on the surface of the magnet mandrel is known as the base curve - the coated conductors are bent along this curve. Bending the coated conductor uniformly along the longitudinal direction in the edge-wise direction is relatively difficult if local kinks are to be avoided. The level of difficulty to wind the coated conductors increase the smaller the diameter of the beam duct. In order to estimate the local bending curvature of the coated conductors, differential geometry is applied [24], [25].

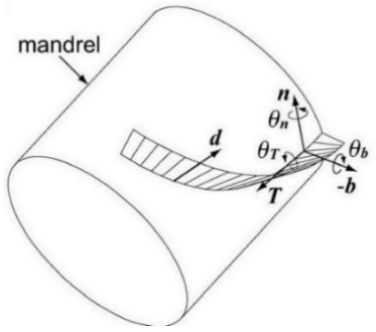

Fig. 2 Conceptual view of three-dimensional winding [4].

Fig. 2 shows the winding of the coated conductors on the mandrel, where the Frenet frame with the vectors $\boldsymbol{T}$, $\boldsymbol{n}$ and $\boldsymbol{b}$ are described in generalized Frenet-Serret equations as in (8) [24]

$$\frac{d\boldsymbol{T}}{ds} = k_n\boldsymbol{n} - k_g\boldsymbol{b}, \quad \frac{d\boldsymbol{n}}{ds} = -k_n\boldsymbol{T} + \tau\boldsymbol{b}, \quad \frac{d\boldsymbol{b}}{ds} = k_g\boldsymbol{T} - \tau\boldsymbol{n}. \tag{8}$$

From the starting point of bending the distance along the base curve is represented by s. The vector **n** is perpendicular to the tape surface, $\boldsymbol{T}$ corresponds to the tangent of the base curve, and $\boldsymbol{b}$ is perpendicular to $\boldsymbol{n}$ and $\boldsymbol{T}$. Torsion, normal curvature and geodesic curvature is represented by τ, k_n and k_g.
The base curve is first to be considered when designing the coil ends. k_g is assumed to be zero, thus allowing $\boldsymbol{b}$, $\boldsymbol{n}$, $\boldsymbol{T}$, τ and k_n to be calculated from (8). It is important that the ends match the magnet cross section that was previously determined through 2D field calculations. For this to be achieved additional twist is applied around $\boldsymbol{T}$. The additional twist does however introduce some geodesic curvature. Thus, a triad of new curvatures, k_g^*, τ^*, and k_n^*, and a new triad of vectors, $\boldsymbol{n}^*$, $\boldsymbol{T}^*$ and $\boldsymbol{b}^*$ are introduced. The curvature parameters are calculated along every coated conductor at each discretization point. The new curvatures and vectors can be calculated using [24]

$$\boldsymbol{T}^* = \boldsymbol{T}, \tag{9}$$

$$\boldsymbol{n}^* = cos\theta_{\boldsymbol{T}}^*\boldsymbol{n} + sin\theta_{\boldsymbol{T}}^*\boldsymbol{b}, \quad \boldsymbol{b}^* = cos\theta_{\boldsymbol{T}}^*\boldsymbol{b} + sin\theta_{\boldsymbol{T}}^*\boldsymbol{n}, \tag{10}$$

$$\tau^* = \tau + d\theta_{\boldsymbol{T}}^*/ds, \tag{11}$$

$$k_g^* = sin\theta_{\boldsymbol{T}}^* k_n, k_n^* = cos\theta_{\boldsymbol{T}}^* k_n. \tag{12}$$

The geodesic curvature is then used to determine the edge-wise bending strain using [4]

$$\varepsilon_g = \left\{\left(\frac{\omega}{2}\right) - \delta\right\} / \left\{\left(\frac{1}{k_g}\right) - \left(\frac{\omega}{2}\right)\right\}, \quad (13)$$

where k_g is edge-wise bending curvature, ω is the width of the tape, and δ is the distance between a point on the tape face and the base curve.
The edge-wise bending strain was set to be less than or equal to 0.3%, and the flat-wise bending radius at minimum 20 mm [26], [27].

IV. Electromagnetic Design Results and Analysis

A. Cross-Section Design of Superconducting Combined Function Magnet

The HTS combined function magnet was designed using the design specifications seen in Table I. The mandrel has a radius of 50 mm, and the straight section length is 1 m.
Fig. 4 shows the steps followed to design the HTS combined function magnet, layer by layer. To achieve the required bending and focusing components the magnet was designed with left-right asymmetry. The continuous ideal surface current distribution around the mandrel for the innermost layer is shown in Fig. 3, and was calculated based on the dipole and quadrupole requirement of 2.88 T and 9.0 T/m. The continuous ideal surface current distribution was then converted into discrete current blocks. These blocks, shown as red blocks in Fig. 5, show the location of the arrangement of the coated conductors, from first to last layer.
Trailing edge PWM is applied to determine the positions of the coated conductors in the same way as in [14]. It is a method to check the amount of surface current required and position coated conductors. The PWM applied can chop the current curves into discrete parts. Each part represents the specific amount of current required to generate designed magnetic fields. The number of coated conductors can be calculated based on this current. This method did however result in an uneven number of tapes carrying positive and negative current in each layer; thus, this was considered in the design of the combined function magnet to ensure there were an equal number of tapes on the left- and right-hand side of the magnet.
With the aim of achieving the required field strength and gradient whilst using less turns of coated conductor, through an iterative process, the blocks positions were placed to achieve a high field homogeneity in the reference radius of the magnet. Once the arrangement of the coated conductor blocks had been determined for the first layer, the harmonic multipole components at the magnet center was calculated, as discussed in section II.

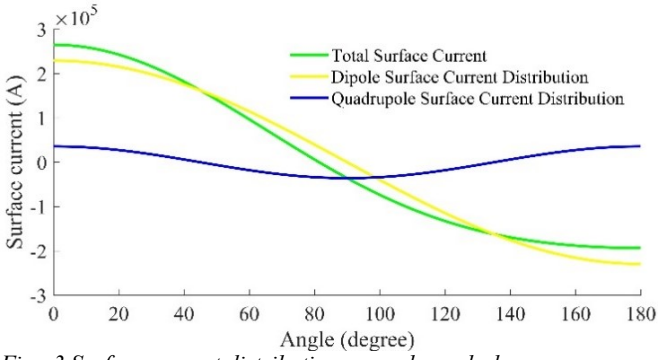

Fig. 3 Surface current distribution around mandrel.

For the next layer, a new surface current was calculated based on the harmonic multipoles generated in the previous layer. This process was repeated until the required magnetic field gradient and strength were achieved.

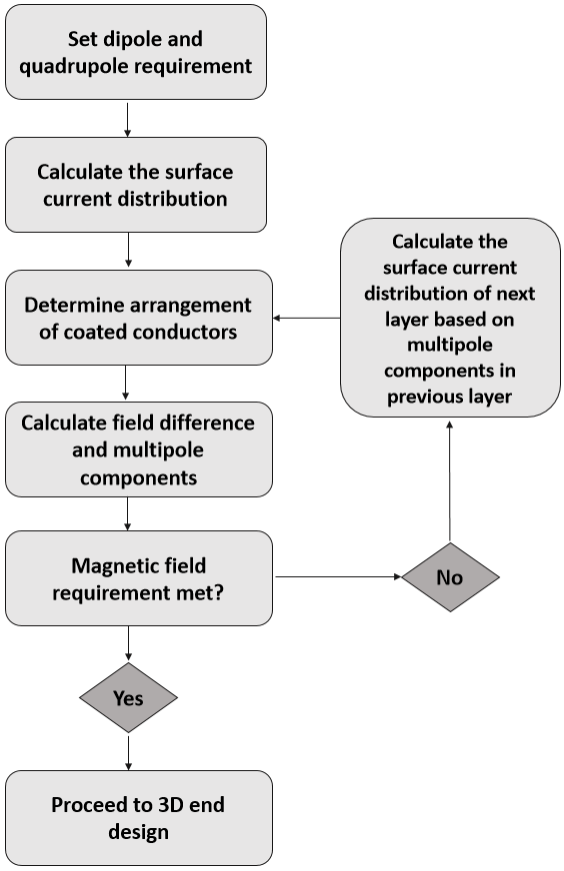

Fig. 4 Flowchart of 2D cross-section design steps.

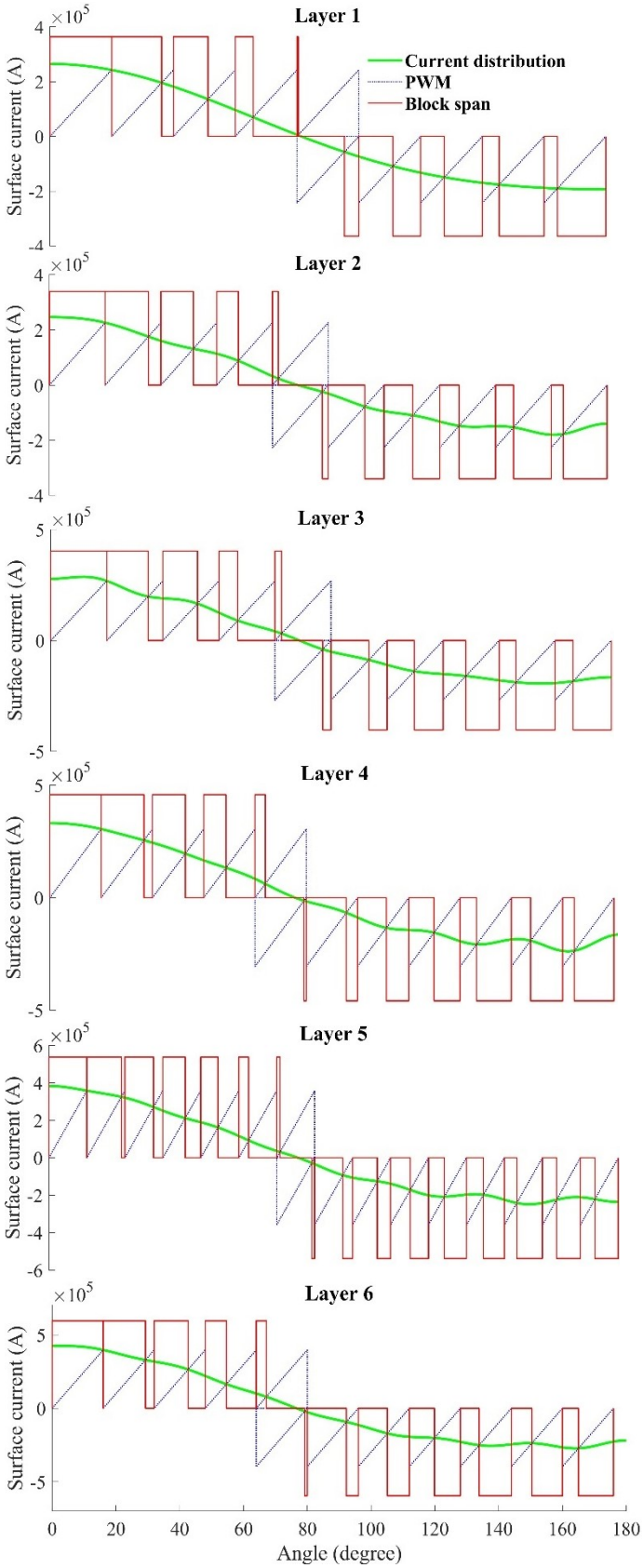

Fig. 5 Trailing edge PWM for magnet cross-section design.

Fig. 5 shows the location of the coated conductors for all the layers, which are represented by the red blocks. The PWM widths for the layers were set to be as wide as possible to reduce the number of blocks, whilst ensuring accuracy was maintained.

The higher harmonic multipole coefficients normalised to the main dipole component at the center of the magnet is shown in Fig. 6. As discussed in greater detail in section III, harmonic coefficients are often used to determine the field quality in the magnet aperture. Fig. 6 shows that the higher multipole components that have been normalised by the dipole component are sufficiently small - smaller than 10^{-4}.

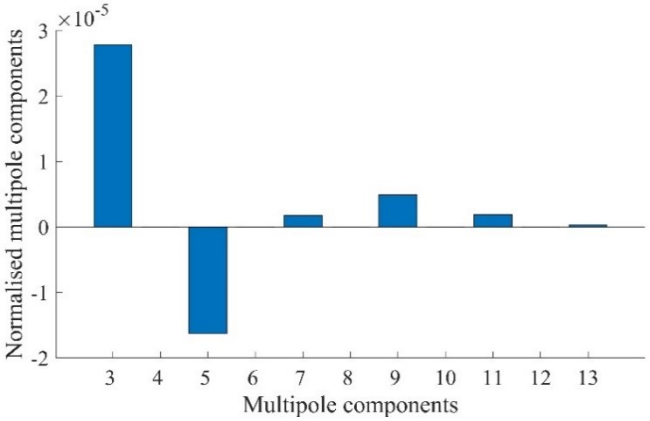

Fig. 6 Multipole components normalised by dipole component at the center of the magnet.

For the innermost layer with a radius of 50 mm, the contribution of the iron yoke of radius 120 mm to the B_1 component was 17% compared to only 0.01% for B_5. Similarly, for the outermost layer with a radius of 85 mm, the contribution of the iron yoke was 50% for the B_1 component compared to 3% for B_5. This shows the importance of optimising the design of the magnet particularly for higher order harmonics as discussed in section III part B.

The HTS combined function magnet cross sectional view is shown in Fig. 7. (left) and is compared to the case study's design shown in Fig 7. (right) [14]. The two designs although noticeably different, are both designed to be vertically asymmetric, but horizontally symmetric, thus coated conductors carrying negative current on the left may connect to different bundles carrying positive current on the right. The case study HTS combined function magnet was not designed with a layer by layer generation, which can be seen from the identical two inner and identical six outer layers.

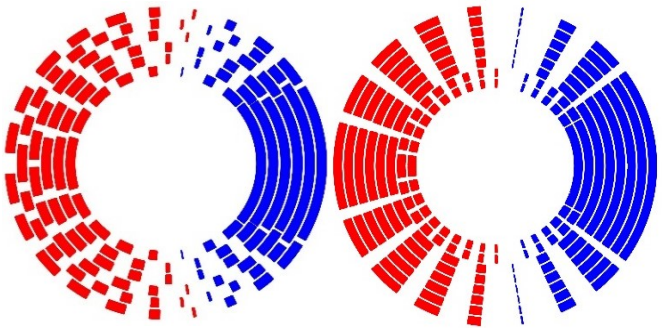

Fig. 7 Left, new HTS layer-by-layer 2D cross-section design, right, existing HTS 2D cross-section design [14].

The bundles of tapes in a layer are stacked around the mandrel's cross-section circumference in a face-to-back stacked position. We assumed coated conductor's thickness and width is 0.2 mm and 5 mm, and the space between stacked tapes set at 0.1 mm; other design specifications are shown in Table I. For each coated conductor it has been assumed that the current flows uniformly across its width. To focus on the layer-by-layer design, similar as previous designs [14], the magnetization current was neglected. The magnetization current is small if charging is done slowly. However, it could be large if currents increase dramatically and special consideration is required. After optimization of the HTS combined function magnet the six layers of coated conductors carrying 200 A each achieved a combined field of 2.93 T and 9.05 T/m, compared to the case study design that achieved 2.88 T and 9.0 T/m with eight layers [14].

B. Coil Ends

The coil ends for the six layers were designed using the theory discussed in section III part C. The optimised cross-section shown in Fig. 7 (left) was used to design the coil ends that are shown in Fig. 8 and Fig. 9.

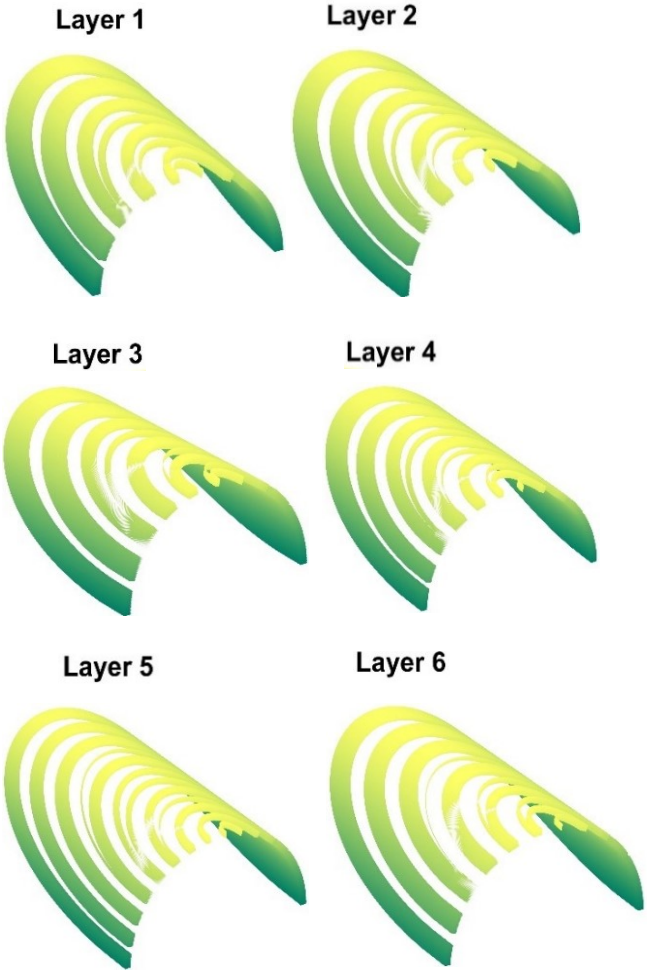

Fig. 8 Coil end design of the layers ranging from innermost layer (Layer 1), second layer (Layer 2) to last layer (Layer 6).

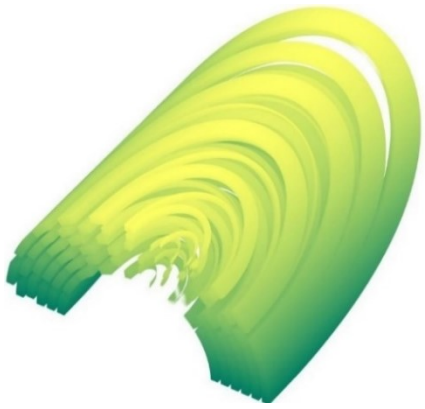

Fig. 9 Coil end design of all layers.

Fig. 10 shows the edge-wise bending strain for the six layers calculated using (13). As seen from the figure, this does not exceed 0.3% for any of the layers. Since some edge-wise bending was allowed in the design, the tapes wide face is parallel to adjacent tapes in the radial section, and almost perpendicular to the mandrel. Flatwise bending radius was calculated from the reciprocal number of curvature and was found to be greater than 20 mm for all tapes in each layer.

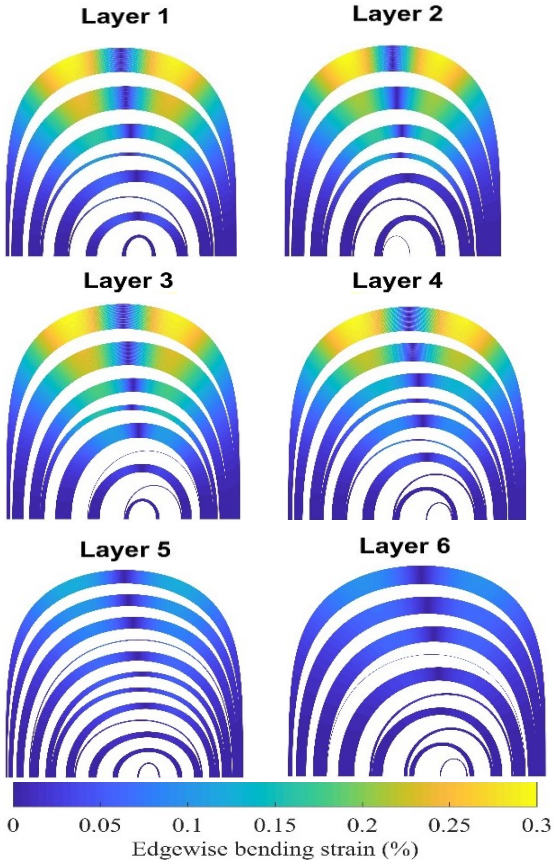

Fig. 10 Edge-wise bending strain for innermost layer (top left), second layer (top right) to last layer (bottom right).

C. Magnetic Field Generation and Analysis of Results

An in house code developed in MATLAB, used the Biot-Savart law to calculate the generated magnetic fields, and the image-current method was used to consider the iron yoke's effect - as discussed in greater detail in section III part B. The

magnetic field generated from the designed HTS combined function magnet across the reference radius of 35 mm is shown in Fig. 11. The figure shows that the design target of 2.88 T is achieved.

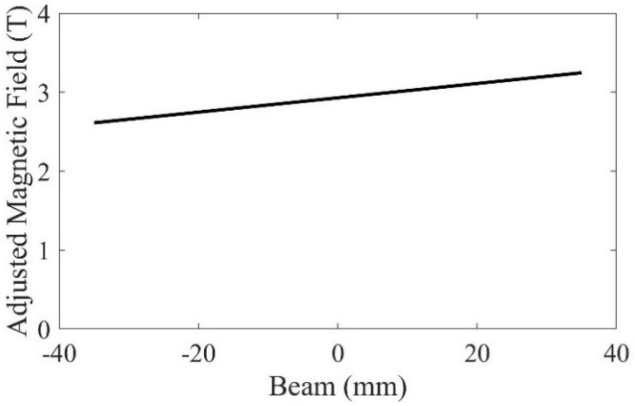

Fig. 11 Magnetic field along the reference radius.

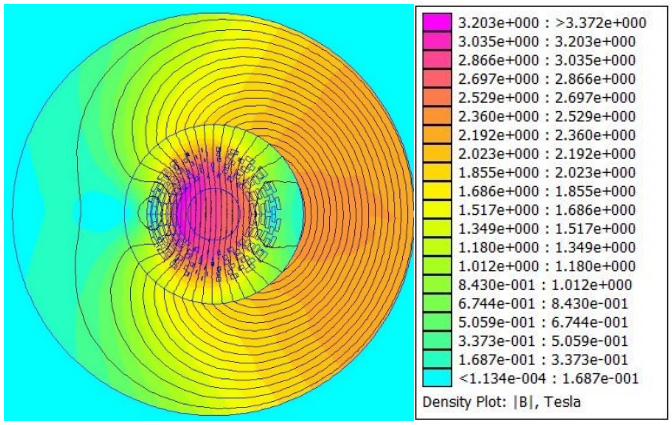

Fig. 12 FEMM Magnetic Flux Density.

To validate the magnetic field calculated using the in house MATLAB code, FEMM version 4.2 [28] was used. The influence of the iron yoke's non-linear effects was considered, using VACOFLUX 50 with a saturation value of 2.3 T [29]. The 2D FEM simulation result is shown in Fig. 12, and shows the magnetic field in the reference radius – represented by the innermost circle in Fig. 12 – corresponds to the magnetic field in Fig. 11. This suggests the iron yoke's non-linear BH characteristics on the magnetic flux density in the reference radius is restrictive. A small area of the iron yoke is saturated, reaching a value of 2.4 T.

Both magnet straight section and coil ends were taken into account when calculating the magnetic field within the reference radius. The magnetic field distribution within the reference radius along the length of the magnet from its center to its coil ends is shown in Fig. 13 and Fig. 14. The colours in Fig. 14 represent the magnitude of the magnetic fields. The designed HTS combined function magnet parameters are shown in Table 2. With a total of 2496 turns using 6472.7 m of coated conductor, the combined function magnet achieved 2.93 T and 9.05 T/m. As seen from Table II, not only did the HTS combined function magnet optimised design achieve the required field strength and gradient, but it did so using a smaller volume of coated conductors compared to the other known design that used 8789.4 m of coated conductor [14].

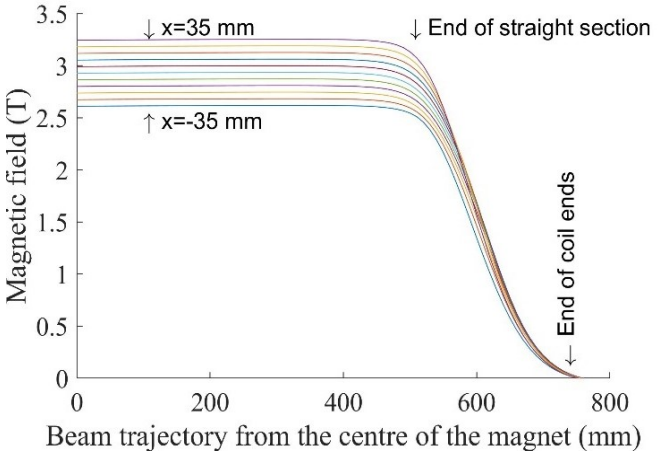

Fig. 13 Magnetic field along the beam trajectory from center to coil ends.

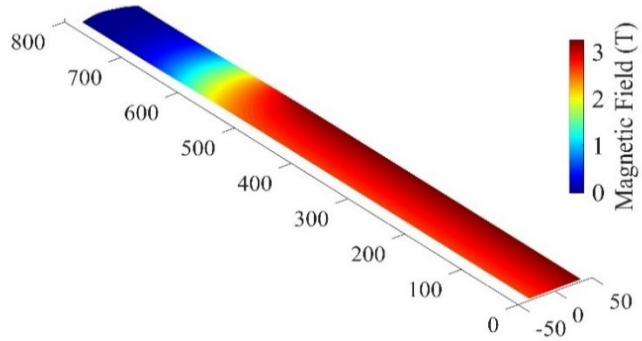

Fig. 14 Magnetic field within the reference radius from center to coil ends.

The shape and outline of the HTS combined function magnet is shown in Fig. 15 and Table II, respectively.

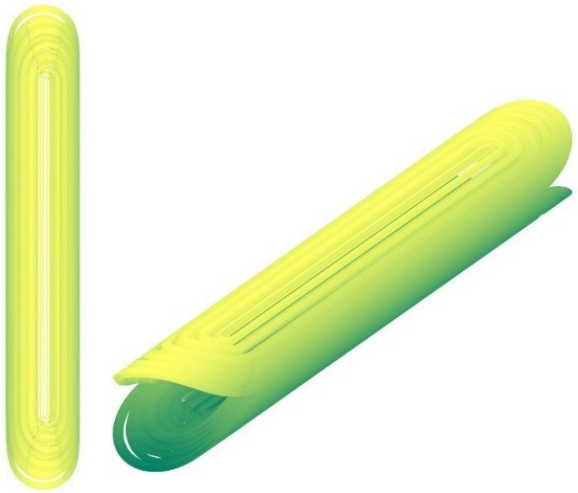

Fig. 15 Three-dimensional shape of the optimised HTS CFM.

TABLE II
MAIN PARAMETERS FOR THE DESIGNED COMBINED FUNCTION MAGNET

Parameter	VALUE	Unit
Straight-section length	500	mm
Radius of each layer		
Layer 1	50	mm
Layer 2	57	mm
Layer 3	64	mm
Layer 4	71	mm
Layer 5	78	mm
Layer 6	85	mm
Number of turns		
Layer 1	336	-
Layer 2	370	-
Layer 3	422	-
Layer 4	422	-
Layer 5	462	-
Layer 6	484	-
Dipole field	2.93	T
Quadrupole field	9.05	T/m
Field uniformity	$<10^{-4}$	-
Conductor length		
Layer 1	816.4	m
Layer 2	903.6	m
Layer 3	1058.7	m
Layer 4	1147.7	m
Layer 5	1209.8	m
Layer 6	1336.5	m
Total length of coated conductor	6472.7	m
Total length of coated conductor compared design	8789.4	m

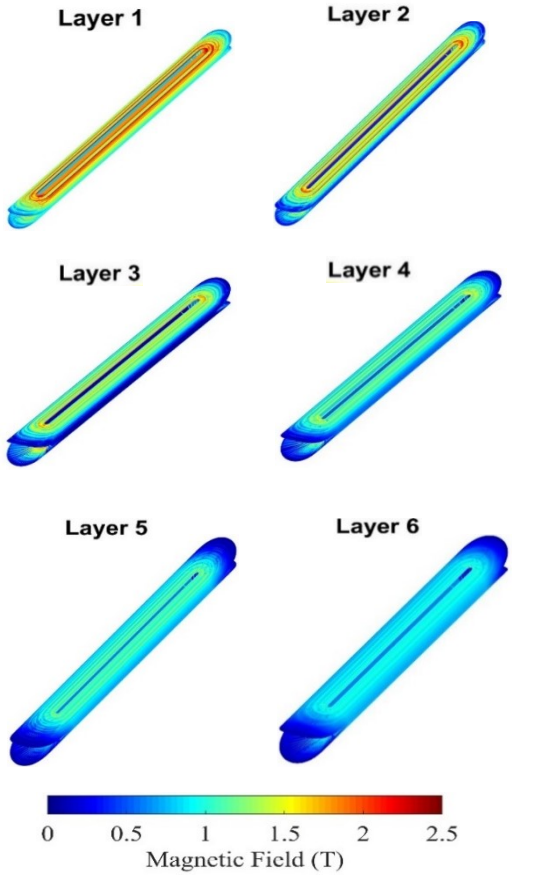

Fig. 16 Magnetic field on tapes from innermost layer (top left), second layer (top right) to last layer (bottom right).

The normal magnetic field on the coated conductor for an operating current of 200A is shown in Fig. 16. As expected, the magnetic field for the innermost layer is the highest.

V. CONCLUSION

A combined function magnet was designed for a rotating gantry for carbon ion therapy. The required dipole and quadrupole functions were achieved, whilst using less coated conductor material compared to the known case study. Mechanical considerations were considered in this design. Henceforth the aim of achieving a more compact magnet with precise magnetic fields was achieved. The next step is to undertake a more detailed analysis along with experimental measurement. Hall sensors will be used to measure the magnetic fields, and harmonic multipole components down to 0.1 mT (around 10^{-4} compared with the dipole component) can be quantified.

VI. REFERENCES

[1] Y. Iwata, T. Shirai and K. Noda, "Design of Superconducting Magnets for a Compact Carbon Gantry," *IEEE Transactions on Applied Superconductivity ,* vol. 26, no. 4, June 2016.

[2] Y. Iwata, K. Noda, T. M. T. Shirai, T. Furukawa, S. Mori, T. Fujita, A. Itano, K. Shouda and K. Mizushima, "Design of a superconducting rotating gantry for heavy-ion therapy," *Physical Review Special Topics - Accelerators and Beams,* vol. 15, no. 4, 2012.

[3] N. Amemiya, H. Otake, T. Sano, T. Nakamura, T. Ogitsu, K. Koyanagi and T. Kurusu, "Temporal behaviour of multipole components of the magnetic field in a small dipole magnet wound with coated conductors," *IOP Superconductor Science And Technology,* vol. 28, no. 3, 2015.

[4] K. Takahashi, N. Amemiya, T. Nakamura, Y. Mori, T. Ogitsu, M. Yoshimoto, I. Watanabe and T. Yoshiyuki, "Magnetic Field Design of Coil-Dominated Magnets Wound With Coated Conductors," *IEEE Transactions on Applied Superconductivity,* vol. 22, no. 3, 2012.

[5] E. Rochepault, P. Vedrine and F. Bouillault, "2D Analytical Magnetic Optimizations for Accelerator Dipole Block Designs," vol. 22, no. 3, June 2012.

[6] Z. Jiang, W. Zhou, Q. Li, M. Yao, J. Fang, N. Amemiya and C. W. Bumby, "The dynamic resistance of YBCO coated conductor wire: Effect of DC current magnitude and applied field orientation," *Superconductor Science and Technology,* vol. 31, no. 3, 2018.

[7] Z. Jiang, W. Zhou, C. Bumby, M. Staines, Q. Li, R. Badcock and N. Long, "Dynamic Resistance Measurement of a Four-Tape YBCO Stack in a Perpendicular Magnetic Field," *IEEE Transactions on Applied Superconductivity,* vol. 28, no. 4, 2018.

[8] Y. Liu, Z. Jiang, Q. Li, C. Bumby, R. Badcock and J. Fang, "Dynamic Resistance Measurement in a Four-Tape YBCO Stack With Various Applied Field

Orientation," *IEEE Transactions on Applied Superconductivity ,* vol. 29, no. 5, 2019.

[9] H. Zhang, M. Yao, Z. Jiang, Y. Xin and Q. Li, "Dependence of Dynamic Loss on Critical Current and n-value of HTS Coated Conductors," *IEEE Transactions on Applied Superconductivity, in press 2019.*.

[10] Q. Li, M. Yao, Z. Jiang, C. W. Bumby and N. Amemiya, "Numerical modeling of dynamic loss in HTS-coated conductors under perpendicular magnetic fields," *IEEE Transactions on Applied Superconductivity,* vol. 28, no. 2, 2017.

[11] M. Pullia and F. Ebskamp, "Introduction to Gantries and Comparison of Gantry Design," 25th November 2016. [Online]. Available: https://indico.cern.ch/event/537685/contributions/2189033/attachments/1379578/2096616/Introduction_to_gantries_and_comparison_of_gantry_design_AIME-SCMED2016.pdf. [Accessed 25th September 2019].

[12] R. Fenning, "Novel FFAG Gantry and Transport Line Designs for Charged Particle Therapy.," Ph.D. dissertation. School of Engineering and Design. Brunel University, London, 2011. Accessed on: Sep. 27, 2019. [Online]. Available: http://citeseerx.ist.psu.edu/viewdoc/download?doi=10.1.1.427.2331&rep=rep1&type=pdf.

[13] K. J. P. e. al., "Conceptual design of a non-scaling fixed field alternating gradient accelerator for protons and carbon ions for charged particle therapy," *Phys. Rev. ST Accel. Beams,* vol. 16, no. 3, p. 030101, 2013.

[14] Q. Li, N. Amemiyaa, T. Nakamuraa and T. Ogitsub, "Magnetic field design of combined-function mangets would with coated conductors," *Physics Procedia,* vol. 45, pp. 237-240, 2013.

[15] S. Russenschuck, "Field Harmonics," in *Field Computation for Accelerator Magnets*, Weinheim, WILEY-VCH Verlag GmbH & Co., 2010, pp. 237-268.

[16] K. Koyanagi, S. Takayama, H. Miyazaki, T. Tosaka, K. Tasaki, T. Kurusu and Y. Ishii, "Development of Saddle-Shaped Coils for Accelerator Magnets Wound With YBCO-Coated Conductors," vol. 25, no. 3, June 2015.

[17] E. Rochepault, P. Vedrine and F. Bouillault, "2D Analytical Magnetic Optimizations for Accelerator Dipole Block Designs," vol. 22, no. 3, June 2012.

[18] S. Russenschuck, "Fields and Potentials of Line-Currents," in *Field Computation for Accelerator Magnets*, Weinheim, WILEY-VCH Verlag GmbH & Co, 2010, pp. 209-210.

[19] N. Amemiya, Y. Sogabe, M. Sakashita and Y. Iwata, "Magnetisation and field quality of a cosinetheta dipole magnet wound with coated conductors for rotating gantry for hadron cancer therap," *Superconductor Science and Technology ,* vol. 29, no. 2, 2016.

[20] Y. Sogabe and N. Amemiya, "AC Loss Calculation of a Cosine-Theta Dipole Magnet Wound With Coated Conductors by 3D Modeling," *IEEE Transactions on Applied Superconductivity ,* vol. 28, no. 4, 2018.

[21] N. Amemiya, H. Miyahara, T. Ogitsu and T. Kurusu, "Design of a cosine-theta dipole magnet wound with coated conductors considering their deformation at coil ends during winding process," *Physics Procedia,* vol. 67, pp. 776-780, 2015.

[22] S. Russenchuck, "Electromagnetic design of superconducting accelerator magnets," CERN European Organization for Nuclear Research, Geneva, 2004.

[23] S. Russenschuck, "Coil-Dominated Magnets," in *Field Computation for Accelerator Magnets*, Weinheim , WILEY-VCH Verlag, 2010, pp. 293-325.

[24] S. Russenschuck, "Differential Geometry Applied to Coil-End Design," in *Field Computation for Accelerator Magnets*, Weinheim, WILEY-VCH, 2010, pp. 609-636.

[25] B. Auchmann and S. Russenschuck, "Coil End Design for Superconducting Magnets Applying Differential Geometry Methods," *IEEE Transactions on Applied Superconductivity,* vol. 40, no. 2, 2004.

[26] D. v. d. Laan and J. W. Ekin, "Dependence of the critical current of YBa2Cu3O7−δ coated conductors on in-plane bending," *IOP Superconductor Science and Technology ,* vol. 21, no. 11, 2008.

[27] M.Sugano, K.Shikimachi, N.Hirano and S.Nagaya, "Simultaneously bending and tensile strain effect on critical current in YBCO coated conductors," *Physica C: Superconductivity and its Applications,* Vols. 463-465, pp. 742-746, 2007.

[28] D. Meeker, "Finite Element Method Magnetics, Version 4.2," Menlo Park, 2018.

[29] VACUUMSCHMELZE GmbH & Co., "49 % Cobalt-Iron-Alloys," VACUUMSCHMELZE GmbH & Co., July 2019. [Online]. Available: https://vacuumschmelze.com/Products/Soft-Magnetic-Materials-and-Stamped-Parts/49-Cobalt-Iron---VACOFLUX-and-VACODUR. [Accessed 2nd October 2019].